# Low-temperature spectroscopic studies of single molecules in 3-D and on 2-D hosts

Smit, R.

# 2

# REVERSE INTERSYSTEM CROSSING IN A SINGLE PERYLENE MOLECULE

*A novel host matrix for perylene, namely dibenzothiophene, is treated in this chapter. Our low-temperature studies on single perylene molecules in this matrix reveal near lifetime-limited emission with a reasonable long-term stability of their spectral lines. Moreover, the resonance fluorescence of perylene molecules reveals an effect that was not observed before at liquid-helium temperatures and with such narrow resonances. Instead of constant depopulation rates for the triplet states, the rates scale linearly with the light intensity of the probe laser, an effect known as reverse intersystem crossing. In this chapter, the observed anomalous behavior of fluorescence blinking will be explained using a model that incorporates all the relevant intramolecular rates. Finally, we show that reverse intersystem crossing helps to improve the stability of the fluorescence signal, which makes perylene competitive in terms of brightness with molecules that are fluorescing more stably in general and thus better approximate a two-level system, such as terrylene and dibenzoterrylene.*

Parts of this chapter have been published in: R. Smit, Z. Ristanovic, B. Kozankiewicz and M. Orrit, 'Reverse Intersystem Crossing of Single Deuterated Perylene Molecules in a Dibenzothiophene Matrix', ChemPhysChem 2022, 23, e202100679

## 2.1. INTRODUCTION

### 2.1.1. MOTIVATION FOR EXPLORING A NEW HOST FOR PERYLENE



Studies of perylene in single-molecule spectroscopy have been largely overshadowed by much brighter emitters, such as terrylene and dibenzoterrylene, that behave more closely to two-level systems. Although perylene has an equally short fluorescence lifetime and an even higher radiative quantum yield than for instance dibenzoterrylene (DBT),[1] the fluorescence signal from a single molecule is less stable due to long-lived triplet states, having extended lifetimes by up to two or three orders of magnitude longer than those of DBT.[2] It is, however, the triplet state and specifically its energy that served as the motivation for this study. If the energy of the triplet state is known, a resonant excitation of the triplet would make it possible to prepare the molecule, on demand, in a state that carries spin, unlike the spin-less singlet states. These studies could be done on a single molecule level, avoiding ensemble-averaging.

There are several methods to acquire the position of the triplet state, for example by recording an absorption spectrum of the $S_0 \rightarrow T_1$ transition or by recording the phosphorescence resulting from intersystem crossing, both performed in ensembles. Several of these attempts have been pursued in our group, for perylene in host matrices, but were unsuccessful. The difficulty of these methods lies respectively in the weak absorption of the $S_0 \rightarrow T_1$ transition and in the low triplet yield of the perylene molecule by intersystem crossing, which is about $10^{-6}$.[3] In other words, 1 million of photons absorbed by a perylene molecule will likely produce a single triplet. Only a tiny fraction of these triplets will actually emit a photon due to a strong internal conversion. This internal conversion rate scales down exponentially with the triplet energy gap, according to the energy gap law.[4] As perylene is the bluest of emitters among the list of terrylene, dibenzoterrylene and others, the internal conversion rate is expected to be the lowest. Considering that we work with fully-deuterated perylene, denoted as perylene-d12, the internal conversion rate is expected to decrease even slightly more,[5] thanks to a weaker vibrationally-assisted relaxation via C-D vibrations, which are about a factor $\sqrt{2}$ lower in energy than C-H vibrations. The afore-mentioned reasons, together with the narrow and relatively stable emission found for perylene at low temperature in some matrices,[3,6,7] rationalizes the choice of perylene for a search for the triplet state's location. However, despite the lower internal conversion, estimates, based on a radiative lifetime in the order of 30 s[8,9] and a triplet lifetime of a few ms,[3] still put the radiative quantum yield of the triplet state of perylene at a low $10^{-4}$. Hence, 10 billion photons absorbed by the singlet of perylene will likely produce a single phosphorescence photon. Only a small fraction of these photons will actually be detected in our setup. In this chapter, we will show that the detection efficiency of our setup is in the order of $10^{-3}$. Finally, a whopping 10 trillion cycles through the singlet manifold would likely give us only one detected phosphorescence photon! This extremely low signal of the phosphorescence makes it exceedingly difficult to detect. Hence, we need some alternative method that particularly bypasses the low triplet yield through intersystem crossing of perylene itself.

We searched for a host matrix that features an increased intersystem crossing rate and hence a higher triplet yield. Yet, these properties must not interfere with measurements

on the guest molecule itself. A first requirement is that the host's singlet excited state must be higher in energy than the singlet excited state of perylene, in order to avoid energy transfer to the host. Studies have also confirmed that a triplet state with a lower energy than the excited singlet state of the guest can lead to intermolecular intersystem crossing, and as a consequence can make fluorescence of a single molecule too weak to detect.[10] Actually, this mechanism, which leads to an enhanced triplet yield of the guest molecules, is at the basis of the only known matrix (anthracene) where phosphorescence of perylene impurities was detected.[6] However, the fluorescence signal of a single molecule was consequently too weak to detect. The second requirement is therefore that the host's triplet state should be higher in energy than perylene's singlet excited state. These two conditions for a host gave us a possible candidate: dibenzothiophene. This chapter will focus on the photophysical studies of perylene in this novel dibenzothiophene matrix, while the follow-up studies on the phosphorescence of perylene in this new matrix will be discussed in the next chapter.

### 2.1.2. THE MATRIX: DIBENZOTHIOPHENE

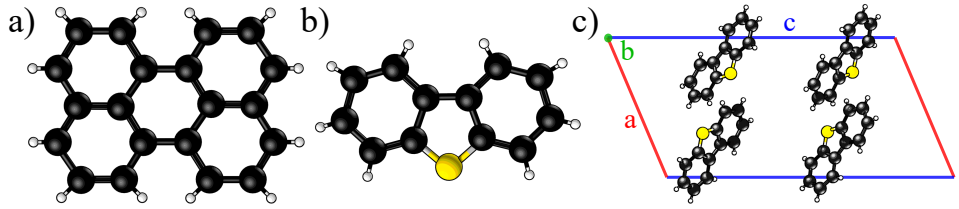


Figure 2.1.: Panel (a) shows the structure of perylene and panel (b) the structure of dibenzothiophene, along with the unit cell of dibenzothiophene in panel (c). The unit cell belongs to the $P_{21/c}$ space group. The insertion of perylene into the dibenzothiophene host matrix is unknown, but the relative sizes of the molecules would likely not permit the removal of more than two dibenzothiophene molecules per perylene guest molecule.

Dibenzothiophene is an organosulfur aromatic compound that consists of two fused benzene rings around a central thiophene unit (Figure 2.1b). Compared to the structurally similar compounds of fluorene, carbazole and dibenzofuran, the dibenzothiophene molecule was found to have a significantly higher ISC rate, which is likely caused by an enhanced spin-orbit coupling due to a heavy-atom effect of the central sulfur atom.[11] The electronic properties of dibenzothiophene have been studied before and it was found that the singlet transition lies around 29,923 $cm^{-1}$ (334.3 nm) and the transition to the triplet at 24,292 $cm^{-1}$ (411.8 nm).[12] This means that both excited states of dibenzothiophene lie well above the singlet excited state of perylene, which was found to be around 446 ± 2 nm in *o*-DCB.[3] In addition, the sizes of perylene and dibenzothiophene do not differ by much, which might make a stable site for insertion into the crystal lattice possible. Moreover, both perylene and dibenzothiophene crystallize according to the same space group: $P_{21/c}$. Despite their similarities, no

previous studies of dibenzothiophene as a host matrix for single molecules have been performed before.



## 2.2. EXPERIMENTAL

### 2.2.1. PREPARATION OF THE MATRIX

Dibenzothiophene was obtained commercially from Alfa Aesar, with a documented purity of about 98%. This starting material was further purified using zone-refining, performed by prof. Boleslaw Kozankiewicz from the Institute of Physics in Warsaw. After a few weeks, colored impurities gathered at the end of the zone-refining tube. Despite that some (colored) impurities were removed, it is known that impurities with a very similar structure to dibenzothiophene, such as phenanthrene, are difficult to remove with zone-refining.[13] A more detailed study of some of the impurities that we found in the zone-refined dibenzothiophene are shown in Chapter 3, which were detected with high sensitivity through their phosphorescence signal.

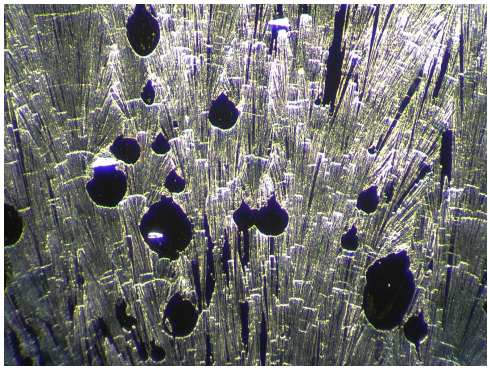

Figure 2.2.: Layer of freeze-quenched polycrystalline dibenzothiophene on a glass cover slip. The preferred crystallization is in the form of needles.

Perylene (Sigma-Aldrich, 98%), in fully-deuterated form, denoted as perylene-d12, was diluted in toluene (Acros Organics, 99.85%). For bulk spectroscopy, a concentration of 10-100 ppm was prepared and for single-molecule experiments the concentration was further decreased to 0.1-10 ppb. Toluene would not be part of the final matrix, but would merely act as a transfer solvent and for a proper control of the concentration and solubility of the guest molecules. The perylene-d12/toluene mixture was pipetted into molten dibenzothiophene (melting point of around 100 ˚C), while the toluene was allowed to evaporate from the hot liquid (boiling point 110.6 ˚C). For bulk spectroscopy, the liquid was subsequently sucked into a heated square borosilicate capillary (VitroTubes, 1 mm ID and 0.2 mm walls) and quickly immersed into liquid nitrogen to avoid expulsion of perylene-d12 from the matrix. For single-molecule measurements, the liquid is pressed between two glass slides to form a thin layer and is again freeze-quenched in liquid nitrogen. The result of this preparation is shown in

Figure 2.2, where a dense configuration of dibenzothiophene needle-shaped crystals can be observed.



### 2.2.2. SETUP

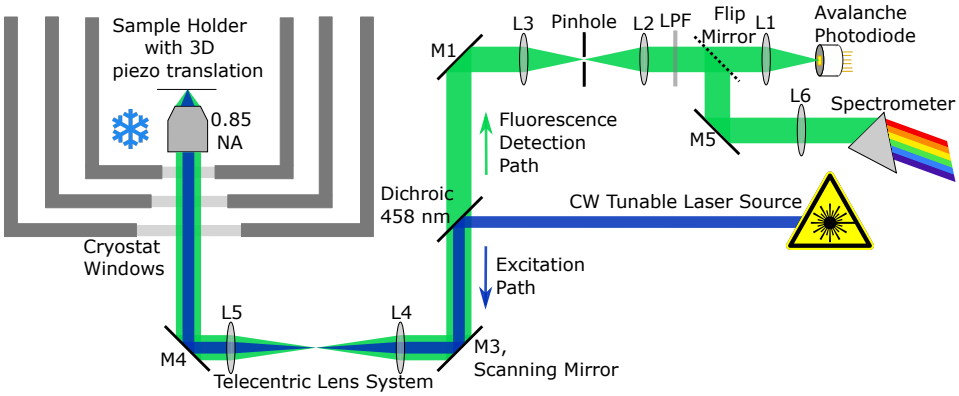


Figure 2.3.: Schematic of the confocal microscope setup used in the experiments. A dichroic separates excitation light from fluorescence and a flip mirror can switch from single-photon detection to the acquisition of spectra.

The samples were measured in a liquid helium flow cryostat (Janis, SVT-200-5) that can reach a working temperature of approximately 1.4 K. With an objective (0.85 NA, Edmund Optics) immersed in liquid helium, the cryostat forms part of a home-built confocal microscope (see schematic in Figure 2.3). A Ti:sapphire laser (M-squared SolsTiS) in combination with a frequency-doubling module (M-squared ECD-X) was used as a narrow bandwidth (< 1 MHz) tunable excitation source, operating in the 440-460 nm range. The output wavelength is monitored continuously with a wavemeter (High Finesse WS6-200), with a resolution of a few MHz. A dichroic mirror (Semrock, FF458-Di02-25x36) is used to separate fluorescence from the excitation light and further spectral filtering is done with a long-pass filter (Chroma, ET460lp). For the full recording of the emission spectrum of perylene-d12 we used a beam splitter instead of a dichroic mirror and made use of a 450 nm long-pass filter (Thor Labs, FEL0450) to remove the excitation light. The laser beam was scanned over the sample by a scanning mirror (Newport, FSM-300-01) and fluorescence was detected by an avalanche photodiode (Excelitas, SPCM-AQRH-16). Fluorescence spectra were recorded with a Horiba iHR320 spectrometer coupled to a liquid-nitrogen-cooled Symphony II CCD detector. The excitation intensity was measured with a power meter (Newport 1830-C), before the laser beam entered the cryostat.

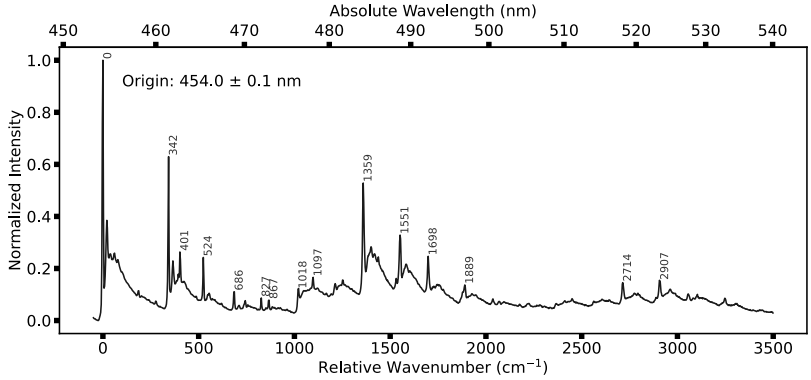


Figure 2.4.: Normalized fluorescence spectrum of an ensemble of perylene-d12 molecules in a dibenzothiophene crystal, measured at a temperature of 1.4 K. The origin of the emission is from the 0-0 zero-phonon line at 454.0 ± 0.1 nm. Some of the most prominent vibrational peaks are annotated. The excitation wavelength was 447.2 nm.

## 2.3. RESULTS AND DISCUSSION

### 2.3.1. ENSEMBLE SPECTROSCOPY

In the first experiment, we illuminated a capillary with perylene-d12-doped dibenzothiophene crystals to observe if there was fluorescence line-narrowing in the emission spectrum at low temperature. The recorded ensemble emission spectrum of perylene-d12 in the matrix, excited with a wavelength of 447.2 nm, is shown in Figure 2.4 and displays a narrow distribution of 0-0 zero-phonon lines (the peak at the origin of the spectrum), together with the vibrational fingerprint that can be attributed to perylene-d12, whose spectrum has been well-studied.[14–17] The origin of the main site is located at 22033 ± 5 cm$^{-1}$ (or 454.0 ± 0.1 nm) with an inhomogeneous broadening of approximately 10 ± 1 cm$^{-1}$. Only a single spectroscopic site is found in the emission spectrum at the chosen excitation wavelength. Other sites may exist, although none are visible in the spectrum of Figure 2.4, probably because these sites have no vibronic transition that coincides with the chosen excitation wavelength. The tunable range of the second harmonic, generated by the laser crystal, is merely 1 nm and for extended scans the angle of the crystal has to be readjusted manually. We also excited the host/guest matrix with a 405 nm laser, but the spectrum is complicated by an overlap with the phosphorescence spectrum of dibenzothiophene and possibly other impurities. Hence, we could not formally identify any other sites. However, with a tunable diode laser, used in the experiments of Chapter 3, we could identify close-by spectroscopic sites and they will be presented in the corresponding chapter.

As the main spectroscopic site is known from the ensemble spectrum in Figure 2.4, single molecules in the inhomogeneous band can be excited selectively with a

narrowband tunable laser and studied one-by-one.

### 2.3.2. SINGLE-MOLECULE STUDIES



The laser, used for ensemble spectroscopy, is also used for a resonant excitation of single molecules. However, we use a different crystal for the generation of the second harmonic, adjusted for the region around 454 nm. The confocal fluorescence images of thin crystals, shown in Figure 2.5a and 2.5b, show why it is necessary to freeze-quench the molten host molecules when doped with guest molecules. In samples that were freeze-quenched, the crystals showed a homogeneous distribution of isolated fluorescent spots (Figure 2.5b), whose activation strongly depends on the excitation frequency. In non-freeze-quenched samples, the fluorescence concentrates at the boundary of the crystals (Figure 2.5a), while the fluorescence signal itself was activated by a wider range of laser frequencies. The slow freezing of molten dibenzothiophene leads to the expulsion of perylene from the matrix, which is of course at the very core of the zone-refining technique, used to extract impurities.

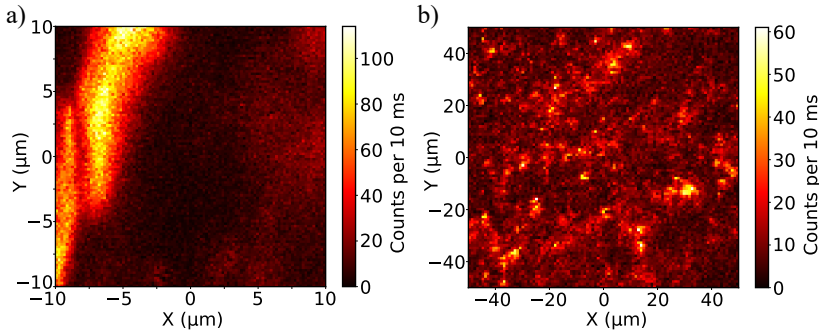


Figure 2.5.: Confocal fluorescence images that show the difference between non freeze-quenched crystals in panel (a) and freeze-quenched crystals in panel (b). In rapidly-frozen crystals, the expulsion of perylene to the boundaries of the crystals is prevented. The quenching results in a homogeneous distribution of molecules, visible as isolated spots. The concentration in both samples is relatively high and the measurement temperature is around 1.4 K.

The sample in Figure 2.5b is still very crowded with single molecules, which leads to a relatively strong background signal, while many molecules are observed in a scan range of 10 GHz. A further reduction of the concentration led to well-isolated single molecules in frequency space. This isolation made it possible to excite a single molecule using a (broad) vibronic transition around 447.1 nm (at the combined energy of the 0-0 ZPL and of the 344 $cm^{-1}$ stretching mode) and record a full emission spectrum, as shown in Figure 2.6. From the ratio of the intensity of the 0-0 ZPL as compared to the combined intensity of the 0-0 ZPL and the phonon-side band (PSB), excluding vibrational peaks, we estimate the Debye-Waller factor to be around 0.40 ± 0.05.

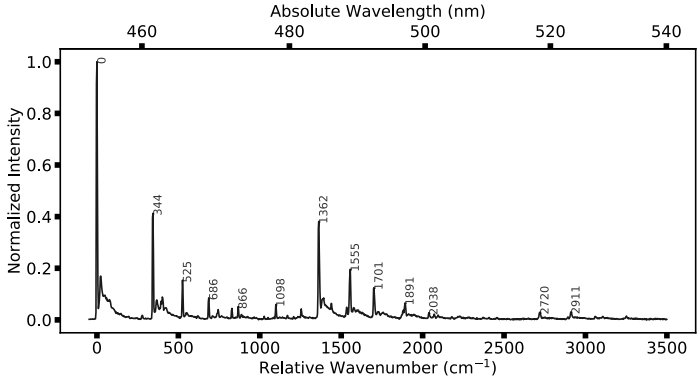


Figure 2.6.: Emission spectrum of a single molecule excited at 447.1 nm by a vibronic transition, given by the energy of the 0-0 ZPL and the 344 cm$^{-1}$ vibration. The spectrum is recorded with a 1200 lines/mm grating and 0.1 mm slit size.

With a resonant excitation of the 0-0 ZPL, we followed single molecules for longer time to observe their frequency stability. Three examples of these time-resolved excitation spectra are shown in Figure 2.7. Here, the background is close to the dark count level of the detector, as the concentration of molecules was very low (1 per 10 GHz range around the center of the inhomogeneous band). At higher concentrations (>1 molecule per 10 GHz around the center of the inhomogeneous band) of molecules, the background was substantially stronger, which is likely fueled by the excitation of ill-inserted and/or spectrally-diffusing molecules. Nonetheless, apart from some small amount of spectral diffusion in Figure 2.7c, most molecules are in general stable. The inhomogeneous coloring of each trace does reveal a strong photoblinking of the fluorescence, related to intersystem crossing to the relatively long-lived triplet state.

For the remainder of this paragraph, the single-molecule measurements will focus on a model molecule for the studied system, denoted as molecule M1. At a low energy excitation, avoiding power-broadening of the spectral line, the linewidth of molecule M1 is found to be around 58 MHz, which is obtained from the Lorentzian fit to the data in Figure 2.8a. Note that the data points in Figure 2.8a are an average of ten single excitation spectra and thus laser jitter and/or spectral diffusion might contribute to the broadening of the measured linewidth. The averaging was necessary to obtain a clear Lorentzian distribution, as single excitation spectra displayed random shapes due to stochastic intersystem crossing, where dwell times in the triplet state could easily exceed the integration time of about 10 ms. The same averaging procedure was followed for the molecule excited at a wide range of laser intensities. The extracted linewidths show the expected broadening with excitation intensity and from the equation in Figure 2.8b, the saturation intensity could be extracted, and was estimated to 22 ± 3 W/cm$^2$ at the focal point.

The homogeneous linewidth of 58 MHz, about the narrowest linewidth found in this

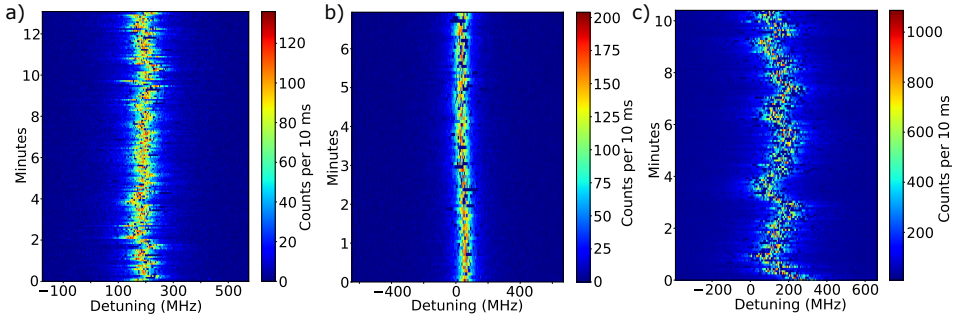


Figure 2.7.: Time-resolved excitation spectra of the 0-0 ZPL of single perylene-d12 molecules. The laser wavelength was monitored continuously using the wavemeter and laser drifts have been corrected, but some jitter in the laser's wavelength might still be present. The molecules show different degrees of stability. The blinking of fluorescence is also clear due to the chosen color scale.

matrix, is slightly broader than what was found for perylene in the Shpol'skii matrix *n*-nonane, where the distribution of linewidths revealed linewidths down to 28 MHz. However, the linewidths are very similar to observations for perylene in *o*-DCB.[3] To determine whether these linewidths were limited by the lifetime of the excited state, we recorded fluorescence decays under a pulsed excitation at 392 nm. These decays were measured for both hydrogenated perylene (Figure 2.9a) and perdeuterated perylene (Figure 2.9b). The difference in the resulting lifetimes is striking, showcasing an increase of the lifetime by about one quarter when all hydrogens are replaced by deuterons. The difference might be explained by a weaker internal conversion, assisted by reduced Franck-Condon factors due to the lower energy of the CD-vibrations as compared to the CH-vibrations.[9] The fluorescence lifetime for perylene-d12 points to a lifetime-limited linewidth of 34.3 ± 0.5 MHz, which is indeed smaller than the measured 58 MHz. Hence, there might be some broadening due to dephasing and/or spectral diffusion, while, as mentioned before, also laser jitter might contribute to the broadening.

Measurements at high excitation intensities reveal anomalous behavior. Close to the saturation intensity of the molecule, the photoblinking of the fluorescence is clearly resolved. Without the afore-mentioned averaging, a single excitation spectrum would show many events where the molecule turned dark, as can be observed in Figure 2.10a, where many points lie between background level and the border of a Lorentzian profile. At high laser intensities, beyond the saturation intensity, the fluorescence signal in Figure 2.10b stabilizes without a single point dropping to background level. As the molecule is saturated, the rate of intersystem crossing should likewise saturate and a lot of blinking should be observed. A possible explanation for the reduced blinking times is reverse intersystem crossing (abbreviated as rISC). In the next paragraph we will use a model that includes rISC to explain the light-induced reduction of the triplet lifetimes. With

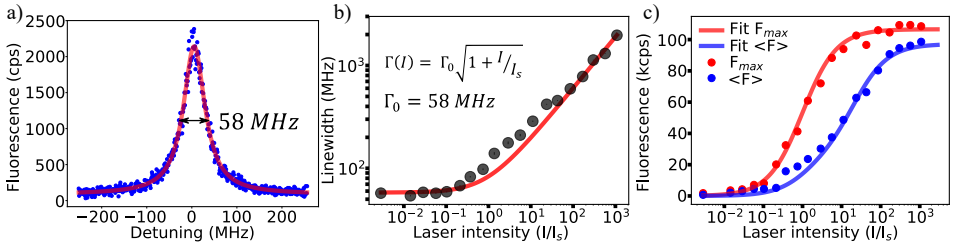


Figure 2.8.: Measurements of molecule M1. Panel (a) shows the averaged line shape of 10 single excitation spectra of a single molecule at 2% of the saturation intensity. The data points have been fitted to a Lorentzian distribution and this yields a full-width-at-half-maximum or homogeneous linewidth of 58 MHz. Panel (b) shows the measured linewidths at a broad range of laser intensities to observe the power broadening of the linewidth. The saturation power that was acquired from the fit is 0.35 ± 0.04 µW, which leads, when taking into account additional power losses before the light enters the objective, to a saturation intensity of 22 ± 3 W/cm$^2$. Strong blinking of the molecules' fluorescence at middle-range powers attributed to an increased uncertainty of the Lorentzian fits, that together with additional broadening due to laser jitter and/or spectral diffusion, probably caused these points to deviate from the fitted line. Panel (c) shows red data points that represent the maximum fluorescence intensity recorded from the molecule at the specified laser intensity, in the cases the fluorescence signal was not or negligibly affected by triplet blinking. The blue data points do take the stochastic intersystem crossing into account and thus represents the average fluorescence signal at a given excitation intensity. The fits will be discussed in paragraph 2.3.3.

this model we will also explain the not yet discussed fit to Figure 2.8c, where it can be noticed that the average fluorescence signal approaches the maximum fluorescence signal that can be obtained from the molecule in case there would be no blinking within the measured time interval.

### 2.3.3. A MODEL FOR THE ENHANCED BRIGHTNESS OF SINGLE MOLECULES

Clear evidence of a reduced triplet lifetime is shown in fluorescence time traces, such as in Figure 2.11. The same time period, but acquired with a large difference in laser intensity yields totally different patterns in the fluorescence blinking. While at low laser intensities compared to the saturation intensity, the pattern shows long periods where the molecule remains dark, a higher laser intensity leads to strongly reduced dark times. In many cases the molecule returns to the bright state within the integration time of 1 ms.

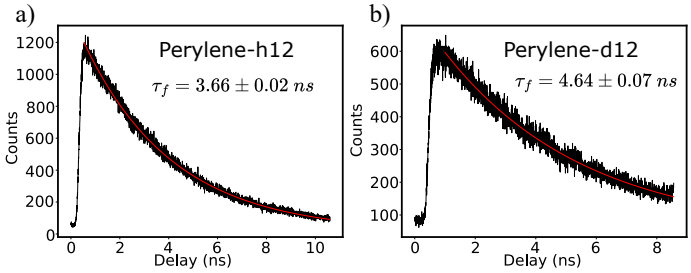


Figure 2.9.: Fluorescence decays of ensembles of perylene-h12 in panel (a) and perylene-d12 in panel (b), both recorded in a dibenzothiophene matrix. The data points fit well to a single exponential decay in both measurements. The excitation wavelength is 392 nm. The data was recorded by prof. Boleslaw Kozankiewicz from the Institute of Physics in Warsaw.

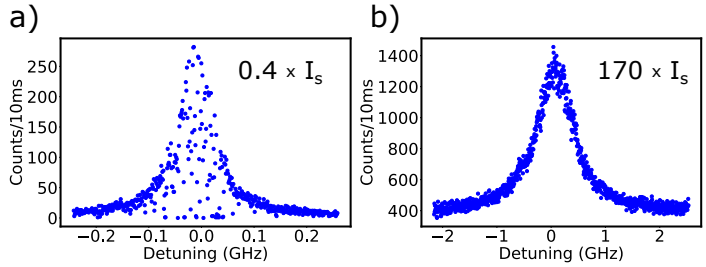


Figure 2.10.: Single excitation spectra of the 0-0 ZPL of molecule M1 at 40% of the saturation intensity in panel (a) and 170 times the saturation intensity in panel (b). Note that in (a) the shape of the Lorentzian is visible at the outer borders, but many points drop below this outer border and some all the way to the background, a signature of blinking. The highest point represents a red data point in Figure 2.8c.

The dynamics of fluorescence blinking can be studied in two ways. If the fluorescence signal is strong enough compared to the background, a threshold level between the on and off state can be determined. The on and off times can then be distributed and fitted to exponential decay(s).[18] The characteristic off time(s) will equal the triplet lifetime(s), while the on times will change with the level of saturation of the molecule. However, at low excitation intensities the signal-to-background ratio is typically very low and at high excitation intensities the background can be strong. In addition, the reduced triplet lifetimes make it harder to distinguish between on and off periods. A powerful tool that overcomes these problems is the autocorrelation of the fluorescence signal, taken at resonance with the 0-0 zero-phonon line. The autocorrelation of the resonance-fluorescence signal can be equated to the second-order intensity correlation function as follows:

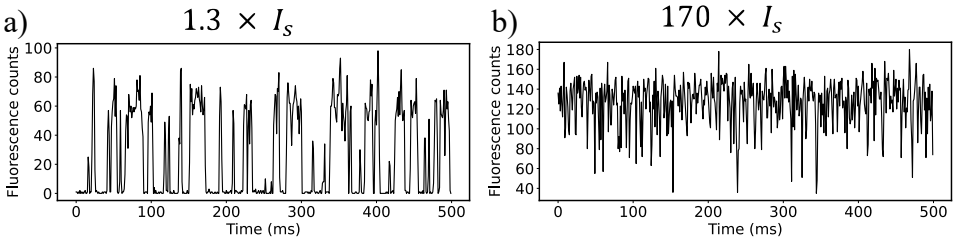


Figure 2.11.: Fluorescence time traces of molecule M1 over a time span of 500 ms, with a 1 ms integration time per point. A significant change in blinking dynamics can be observed between panel (a) representing a low excitation intensity and panel (b) a high excitation intensity. The reduction in dark times can be explained by a change in the triplet lifetime due to reverse intersystem crossing.

$$g^{(2)}(\tau) = \frac{< I(t)I(t+\tau)}{< I(t) >^2} \tag{2.1}$$

Time series, such as in Figure 2.11, were recorded with an integration time of 10 µs for a period of 60 s up to 120 s. The length of the series was enough to have a relatively good signal to noise ratio in the autocorrelations, while restricting file sizes to 100-200 MB. The recorded time series were autocorrelated for time delays up to 1 second. This resulted in an exponentially decaying time dependence (Figure 2.12).

From the rate equations and their solutions (see reference[3]) we fitted the autocorrelation $g^{(2)}(\tau)$ in equation 2.1 to:

$$g^{(2)}(\tau) = C_0 + C_1 e^{-\lambda_1 \tau} + C_2 e^{-\lambda_2 \tau} \tag{2.2}$$

The fitting of both exponentials worked well for autocorrelations obtained at low excitation intensities, although the contrast of the long-lived decay is very low compared to the short-lived decay (Figure 2.12a). With laser intensities above saturation it becomes increasingly difficult to fit to a combination of two exponential decays and at the highest intensities, the autocorrelation fits very well to a single exponential decay, as in Figure 2.12c. The parameter $C_0$ is in most cases very close to 1, which indicates that the autocorrelation is not significantly affected by stray correlations. However, mechanical vibrations of the vacuum pump coupling to the sample holder left a fingerprint in the autocorrelation, with a characteristic frequency of 100 Hz. To correct for this, we measured an autocorrelation of a background signal and divided out these contributions to the autocorrelation functions in equation 2.2. This correction has been done already for the autocorrelation curves in Figure 2.12. Apart from corrections arising from these mechanical vibrations in our setup, the contributions from the background need to be corrected as well, which affects the contrasts of the exponential decays.[19] Corrections for the background-to-signal ratio can be taken into account by multiplying the individual

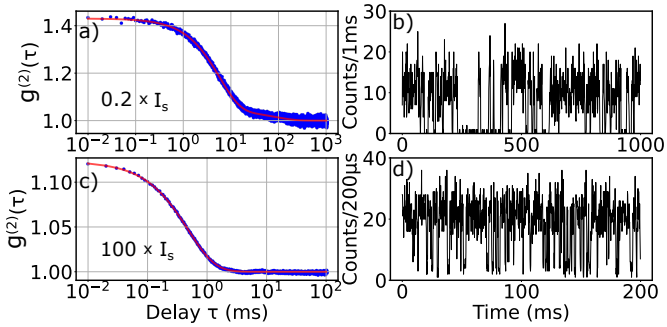


Figure 2.12.: Fits of the autocorrelation curves (left) and parts of the corresponding fluorescence time traces (right) of molecule M1 at a low excitation intensity of 20% of the saturation intensity in panel (a) and panel (b) and 100 times the saturation intensity in panel (c) and (d). Note that the time scales in (a) and (c) differ, while also the integration time for (b) is 1 ms and 200 $\mu$s for (d). In addition, the fit in (a) is a sum of two exponentials, while (c) was fitted to a single exponential decay.

fits to equation 2.2 through a prefactor: $(1+\frac{B}{S})^2$, where $B$ is the background signal compared to the molecules' signal $S$. Hence, for each excitation intensity this $\frac{B}{S}$ ratio has to be determined. In general, the background never exceeded 40% of the total signal for the highest excitation intensity that was used in the experiments.

The existence of two well-separated exponential decays at low excitation intensities points to a distinguishability of two out of three triplet substates. Typically, the short-lived decays are attributed to the $T_x$ and $T_y$ substates, while the longer-lived decay is assigned to the $T_z$ state.[20] The rate equations assign two rates for each of the two sets of substates - which we will distinguish with the labels xy and z - namely a population rate and a depopulation rate. The population rate of the triplet states is determined by the intersystem crossing rate and will be denoted as $(k_{23}^{xy}, k_{23}^{z})$, see diagram in Figure 2.13. Since the population rate of the triplet state is affected by the level of saturation of the molecule, we will denote these as the effective ISC rates. These rates can then be expressed in terms of the intrinsic ISC rates $(\gamma_{23}^{xy}, \gamma_{23}^{z})$ and of the excitation intensity as:

$$(k_{23}^{xy}(I), k_{23}^{z}(I)) = \frac{(\gamma_{23}^{xy}, \gamma_{23}^{z})}{2} \frac{\frac{I}{I_s}}{1+\frac{I}{I_s}}. \tag{2.3}$$

A populated triplet state will also be depopulated with a characteristic rate, which will be denoted as $(k_{31}^{xy}, k_{31}^{z})$. In general, these rates are assumed to be independent of the excitation intensity, but surprisingly that is not the case for this host/guest matrix. Hence, at this point, the model will start to deviate from the standard model and we will include a rISC term. Similar to the ISC rates, the triplet depopulation rates will be denoted as the effective depopulation rates. However, there must be a power-independent intrinsic

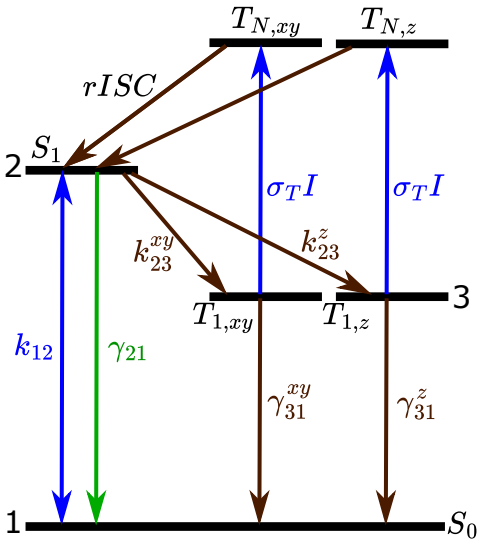


Figure 2.13.: Jablonski diagram of the energy level structure of perylene-d12. The intramolecular rates between the relevant energy levels are displayed next to the corresponding arrow of the transition. rISC is here depicted as a transition between $T_1$ and a higher excited triplet state $T_N$, of which the index is not known, followed by intersystem crossing back to the singlet excited state. The transition from $T_1$ to $T_N$ is shown here with its associated absorption cross section $\sigma_T$, while the whole process of rISC will be captured by $\alpha$ (see equation 2.4).

depopulation rate, in case there is no contribution from rISC. The intrinsic depopulation rates will be called $(\gamma_{31}^{xy}, \gamma_{31}^{z})$. To model the triplet depopulation rates on excitation intensity, a rISC term, $\alpha$, is added as a secondary channel for the depopulation of the triplet state. We assume $\alpha$ to be the same for all three triplet sublevels. The effective depopulation rates will then become linearly-dependent on the light intensity:

$$(k_{31}^{xy}(I), k_{31}^{z}(I)) = (\gamma_{31}^{xy}, \gamma_{31}^{z}) + \alpha I. \tag{2.4}$$

Finally, using the standard model for the population rates, with the added rISC term in equation 2.4, we can describe the contrasts $C_1$ and $C_2$ and the decay parameters $\lambda_1$ and $\lambda_2$ of equation 2.2 in terms of the effective population and depopulation rates of the triplet states. Starting with the contrasts of the two exponentials, we have the following expression:

$$C_{1,2} = \frac{\lambda_{1,2}(k_{31}^{xy} - \lambda_{1,2})(k_{31}^{z} - \lambda_{1,2})}{k_{31}^{xy} k_{31}^{z}(\lambda_{1,2} - \lambda_{2,1})}, \tag{2.5}$$

where the decay parameters, $\lambda_1$ and $\lambda_2$, are given by solutions of a characteristic equation:

$$\lambda_{1,2} = \frac{1}{2}(\Sigma \pm D), \tag{2.6}$$

with $\Sigma$ the sum of all rates and $D$ the discriminant of the characteristic equation, given by:

$$\Sigma = k_{23}^{xy} + k_{23}^{z} + k_{31}^{xy} + k_{31}^{z}, \tag{2.7}$$

$$D = \sqrt{\Sigma^2 - 4(k_{23}^{xy}k_{31}^{z} + k_{23}^{z}k_{31}^{xy} + k_{31}^{xy}k_{31}^{z})}. \tag{2.8}$$

The cross-dependencies of equations 2.5,2.6,2.7 and 2.8 require that we have to fit all the parameters to the measurements at once. In addition, the dependence of equation 2.3 and 2.4 on respectively the saturation intensity and laser intensity adds more terms to fit. Hence, the equations for the fits in Figure 2.8b and 2.8c are included in the global fit to find the best matching parameters that satisfy the whole set of measurements. As we now have a model for rISC, the fit in Figure 2.8c can be discussed.

In general, the saturation of the fluorescence signal $(F)$ from a single molecule follows a sigmoid-shaped curve, which has the following form:

$$F(I) = F_\infty \frac{\frac{I}{I_s}}{1 + \frac{I}{I_s}}. \tag{2.9}$$

This standard equation for saturation is used to describe the red data points and fit in Figure 2.8c, which traces the maximum fluorescence signal obtained from the single molecule, without blinking due to ISC. The saturation of a three-level system can also be described in terms of all intramolecular rates[21,22]

$$F(I) = \eta \frac{\Phi_F \tau_F^{-1}}{2 + \frac{k_{23}^{xy}}{\gamma_{31}^{xy}} + \frac{k_{23}^{z}}{\gamma_{31}^{z}}} \frac{\frac{I}{I_s}}{1 + \frac{I}{I_s}}. \tag{2.10}$$

The parameter $\eta$ is the detection efficiency of our setup, $\Phi_F$ is the fluorescence quantum yield and $\tau_F$ is the fluorescence lifetime. The fluorescence lifetime was already determined to be around 4.6 ± 0.1 ns using time-correlated single-photon counting under a pulsed excitation (Figure 2.9). A key difference between equation 2.9 and 2.10 is the inclusion of the ISC rates and triplet lifetimes, which are a limiting factor on the total fluorescence output. If the triplet depopulation rates would be constant with excitation intensity, the shape of the function, a sigmoid, would be preserved. However, the linear dependency of the depopulation rates on laser intensity captures the deviation of the saturation curve as observed for the blue points and fit curve in Figure 2.8c. As part of the global fit, we find a detection efficiency of our setup of around $9 \times 10^{-4}$, which is a typical value for our setup when assuming $\Phi_F$ to be close to unity (about 0.89[23]). The relatively low detection efficiency is likely caused by a combination of a low NA objective, a lower quantum efficiency of our detector for the blue part of the spectrum and potential further losses in our cryogenic confocal setup, which is optimized for the near-infrared. Despite the low collection efficiency, the molecule is much brighter due to rISC, than it would have been in the absence of rISC. Based on the intrinsic

depopulation rates, the molecule would have saturated at a low 22 kcps, while with rISC we find a saturation intensity that is at least a four-fold higher, with about 100 kcps.



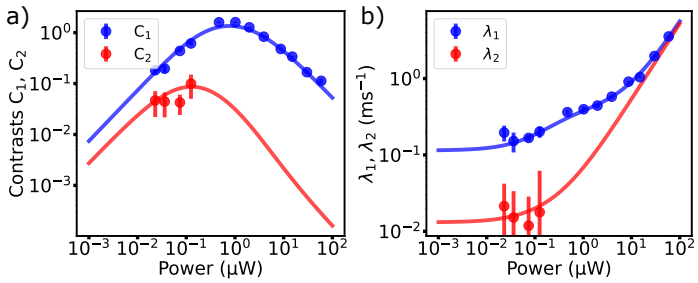


Figure 2.14.: Model fit for molecule M1. The points in panel (a) show the contrasts obtained from the individual fits to the autocorrelation curves, while the line is obtained from the global fit to equation 2.5. For panel (b) the points are given by the decay parameters obtained from the autocorrelation curves, while the line was obtained from the global fit to equation 2.6. Note that for the long-lived decay, the large difference between $C_1$ and $C_2$ from the fifth point and onwards made it difficult to distinguish two decays from the autocorrelation curve. Hence, from the fifth point and onwards we only fitted a single exponential decay.

Before we performed the global fit, all the recorded autocorrelation functions, such as in Figure 2.12, are fitted to equation 2.2 to obtain the contrasts $C_1$ and $C_2$ and decay parameters $\lambda_1$ and $\lambda_2$. The resulting data is subsequently processed in a global fit, using equations 2.5-2.8. The data points for the contrasts and decay parameters and the result of the global fit are shown in Figure 2.14. The fit is logarithmically-weighted with the errors obtained from the individual fits of the autocorrelation curves. The optimal values that we find for the intrinsic population rates $\gamma_{23}^{xy}$ and $\gamma_{23}^{z}$, the intrinsic depopulation rates $\gamma_{31}^{xy}$ and $\gamma_{31}^{z}$ and finally the rISC parameter $\alpha$ are shown in Table 2.1, for molecule M1 and two other molecules.

| | $\gamma_{23}^{xy}(s^{-1})$ | $\gamma_{31}^{xy}(s^{-1})$ | $\gamma_{23}^{z}(s^{-1})$ | $\gamma_{31}^{z}(s^{-1})$ | $\alpha(\mu W^{-1}s^{-1})$ | $I_s(Wcm^{-2})$ | $F_\infty(kcps)$ | $\Gamma_0(MHz)$ | $\lambda(nm)$ |
|---|---|---|---|---|---|---|---|---|---|
| $M1$ | $542 \pm 25$ | $114 \pm 9$ | $23 \pm 6$ | $13 \pm 2$ | $52.3 \pm 0.8$ | $22 \pm 3$ | $106 \pm 1$ | $58 \pm 1$ | 454.57 |
| $M2$ | $550 \pm 70$ | $91 \pm 7$ | $76 \pm 55$ | $15 \pm 11$ | $14.2 \pm 0.6$ | $82 \pm 20$ | $51 \pm 5$ | $55 \pm 2$ | 454.38 |
| $M3$ | $500 \pm 27$ | $146 \pm 11$ | $38 \pm 13$ | $19 \pm 3$ | $26.5 \pm 0.9$ | $59 \pm 5$ | $155 \pm 2$ | $59 \pm 1$ | 454.36 |

Table 2.1.: Reported results of the global fit for three individual molecules, for parameters as described in the text and Figure 2.13. The reported errors are standard deviations from the global fit.

From the intrinsic depopulation rate of the triplet state the triplet lifetime can be determined. For the average of the three molecules we find a triplet lifetime $(\gamma_{31}^{xy})^{-1}$ of the $T_{xy}$ states of 8.5 ± 0.4 ms and for the $T_z$ state a lifetime of 64 ± 12 ms. The average intersystem crossing rates are determined to be 532 ± 26 $s^{-1}$ for the

$T_{xy}$ states and 46 ± 19 $s^{-1}$ for the $T_z$ state. The relatively large uncertainty of the parameters for the long-lived decay in Table 2.1 are likely related to the low photon counts of the measurements at low power, at which we were able to extract information about this state. At higher excitation intensities, the rISC parameter $\alpha$ dominated the statistics. Likely, the dominance of α leads to a convergence of the triplet depopulation rates of the $T_{xy}$ and $T_z$ substates, which causes the two exponential decays to start to overlap, becoming indistinguishable. Other variations between the results in Table 2.1 might be caused by heterogeneity of embedding sites, orientations and defects of the polycrystalline samples. When the rISC parameter $\alpha$ is corrected for the variations in saturation intensity, the average increase of the triplet depopulation rates is about 18 $s^{-1}$ per saturation intensity.

The triplet lifetimes that we find are significantly longer than reported in the literature, i.e. 3.0 ms and 19 ms for non-deuterated perylene in *o*-DCB[3] or 1.1 ± 0.5 ms in *n*-nonane.[7] The increased lifetime is likely caused by the deuteration of the perylene molecule.[24] In general, the triplet lifetimes are reported to be longer for perdeuterated fluorophores compared to their non-deuterated analogues.[24] For perylene-d12 dissolved in PMMA, the triplet lifetime was found to increase by a factor of 2.3 (298 K) compared to perylene-h12.[24] Other parameters, such as triplet yield, are more comparable. From the ISC rate and the fluorescence lifetime we calculate a triplet yield by the equation $\Phi_T = \tau_F(k_{23}^{xy} + k_{23}^{z})$ and we find a value in the order of $3 \times 10^{-6}$, which is equal to the triplet yield found for perylene-h12 in *o*-DCB.[3]

The reason for efficient rISC taking place in this particular matrix, as opposed to other matrices that have been used for perylene or many other guest molecules, remains unknown. Only for terrylene in *p*-terphenyl, rISC was observed at temperatures above 50 K, but was absent or negligible at lower temperatures.[25,26] The most commonly proposed pathway for rISC involves an intramolecular intersystem crossing, i.e., a spin-flip process when the perylene molecule is in a high triplet level.[27,28] In higher excited states, the density of vibrational states in both multiplicities makes it easy to achieve resonance between triplet and singlet levels, leading to relaxation to the lower singlet states. The large $T_1 - T_N$ energy gap and the energetic proximity of $T_N$ and $S_N$ could favor rISC over an internal conversion process from $T_N$ to $T_1$.[28] In addition, this internal conversion could be a bit more suppressed due to the deuteration of the molecule. There might be also a role of the matrix, such as that the relatively heavy sulfur atom of the matrix molecule could further help couple singlet and triplet states, particularly in the more delocalized orbitals of the higher excited states.[29] If this triplet-to-singlet transition is fast enough, the rISC rate would be dominated by the optical excitation of the $T_{xy}$ and $T_z$ states, leading to the same rISC rate for all the three triplet sublevels. Finally, the efficiency of rISC does not appear to vary significantly from molecule to molecule. However, the rISC process could be of use while doing spectroscopic studies on the excited triplet states by not using the optical fluorescence-exciting beam to induce rISC, but by using a secondary tunable beam[27] or a time-gated double excitation method to determine the quantum yields of the $T_N$ to $S_1$ rISC[29] (see scheme in Figure 2.15). The rISC process might also be harnessed for a better control of triplet blinking in view of fluorescence super-resolution STORM schemes at low temperature.[30–32]

## 2.4. CONCLUSION AND OUTLOOK

In this chapter, we have demonstrated that dibenzothiophene is an appropriate matrix for perylene. The spectral lines of perylene are relatively stable and the 0-0 zero-phonon lines have a near lifetime-limited linewidth. Moreover, at higher excitation intensities, the fluorescence signal from single perylene molecules is on par with other bright systems commonly employed as lifetime-limited single-molecule emitters. That is a direct consequence of reverse intersystem crossing (rISC) that allows the recovery of the molecule from the long-lived triplet state and at least quadruples the detectable fluorescence rate. By studying the autocorrelations of fluorescence time traces we were able to estimate the intrinsic triplet lifetimes of deuterated perylene to be 8.5 ± 0.4 ms for the $T_{xy}$-states and 64 ± 12 ms for the $T_z$-state. In addition, we were able to quantify the effect of rISC on the depopulation rate of the triplet states.

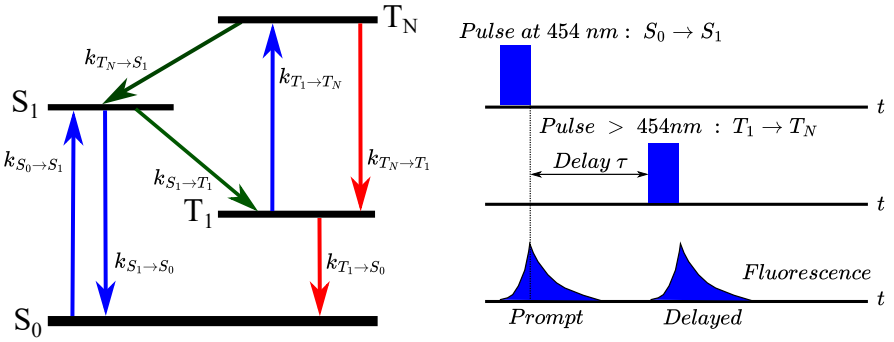


Figure 2.15.: Proposed pump-probe experiment on single perylene molecules or ensembles to determine rISC efficiency as a function of wavelength. The experiment starts with an initial laser pulse tuned to the resonance of the $S_0 \to S_1$ transition. Through intersystem crossing (part of) the molecule(s) end up in the triplet state $T_1$. A second short pulse, off-resonant with the $S_0 \to S_1$ transition and delayed enough for prompt fluorescence to have decayed significantly, is used to probe resonances in the $T_1 \to T_N$ transition. Successful transfer of the population from $T_1 \to S_1$, through $T_N$, would give rise to delayed fluorescence, with near-unity quantum yield. This would in principle allow the measurement of a $T_1 \to T_N$ absorption spectrum as a function of the delayed fluorescence signal obtained through the rISC process. Separation of prompt and delayed fluorescence can be handled using an optical chopper as described in Chapter 3. When the rate of absorption in the triplet, $k_{T_1 \to T_N}$, and the rISC rate, $k_{T_1 \to S_1}$, are known, the non-radiative rate $k_{T_N \to T_1}$ could be determined from experiment.

The demonstrated effect of rISC, never observed at such low temperatures and with narrow resonances, could be used in the future to study the higher triplet states of perylene, by using a second tunable laser beam that probes the rISC efficiency as a

function of $T_1 \rightarrow T_N$ absorption, while similar to studies of anthracenes,[29] a time-gated double-excitation method as described in Figure 2.15, could be used to determine the quantum yields of rISC. Finally, it would be interesting to find out if rISC would be also present in hydrogenated perylene, in order to see if the change in vibrational energies between perdeuterated and hydrogenated perylene is a reason why rISC has never been observed before for perylene in other systems.



In the next chapter, we will proceed with our new host-guest system to find out whether we can detect phosphorescence from the triplet states.

# REFERENCES


(1) Erker, C.; Basché, T. *Journal of the American Chemical Society* **2022**, *144*, 14053–14056.

(2) Nicolet, A. A. L.; Hofmann, C.; Kol'chenko, M. A.; Kozankiewicz, B.; Orrit, M. *ChemPhysChem* **2007**, *8*, 1215–1220.

(3) Verhart, N. R.; Navarro, P.; Faez, S.; Orrit, M. *Physical Chemistry Chemical Physics* **2016**, *18*, 17655–17659.

(4) Englman, R.; Jortner, J. *Molecular Physics* **1970**, *18*, 145–164.

(5) Siebrand, W.; Williams, D. F. *The Journal of Chemical Physics* **1967**, *46*, 403–404.

(6) Walla, P. J.; Jelezko, F.; Tamarat, P.; Lounis, B.; Orrit, M. *Chemical Physics* **1998**, *233*, 117–125.

(7) Pirotta, M.; Renn, A.; Werts, M. H. V.; Wild, U. P. *Chemical Physics Letters* **1996**, *250*, 576–582.

(8) Kellogg, R. E.; Bennett, R. G. *The Journal of Chemical Physics* **1964**, *41*, 3042–3045.

(9) Siebrand, W. *The Journal of Chemical Physics* **1967**, *47*, 2411–2422.

(10) Nicolet, A.; Kol'chenko, M. A.; Kozankiewicz, B.; Orrit, M. *The Journal of Chemical Physics* **2006**, *124*, 164711.

(11) Goldacker, W.; Schweitzer, D.; Zimmermann, H. *Chemical Physics* **1979**, *36*, 15–26.

(12) Bree, A.; Zwarich, R. *Spectrochimica Acta Part A: Molecular Spectroscopy* **1971**, *27*, 621–630.

(13) McArdle, B. J.; Sherwood, J. N. **1974**, *22*, 193–200.

(14) Abram, I. I.; Auerbach, R. A.; Birge, R. R.; Kohler, B. E.; Stevenson, J. M. *The Journal of Chemical Physics* **1975**, *63*, 2473–2478.

(15) Unwin, P. J.; Jones, T. S. *Surface Science* **2003**, *532*, 1011–1016.

(16) Suganuma, Y.; Kowaka, Y.; Ashizawa, N.; Nakayama, N.; Goto, H.; Ishimoto, T.; Nagashima, U.; Ueda, T.; Yamanaka, T.; Nishi, N.; Baba, M. *Molecular Physics* **2011**, *109*, 1831–1840.

(17) Sulkes, M. *Chemical Physics* **1987**, *114*, 289–294.

(18) Basché, T.; Kummer, S.; Bräuchle, C. *Nature* **1995**, *373*, 132–134.

(19) Bernard, J.; Fleury, L.; Talon, H.; Orrit, M. *The Journal of Chemical Physics* **1993**, *98*, 850–859.

(20) Lawetz, V.; Orlandi, G.; Siebrand, W. *The Journal of Chemical Physics* **1972**, *56*, 4058–4072.

(21) De Vries, H.; Wiersma, D. A. *The Journal of Chemical Physics* **1980**, *72*, 1851–1863.

(22) Ambrose, W. P.; Basché, T.; Moerner, W. E. *The Journal of Chemical Physics* **1991**, *95*, 7150–7163.

(23) Birks, J. B.; Dyson, D. J.; Flowers, B. H. *Proceedings of the Royal Society of London. Series A. Mathematical and Physical Sciences* **1963**, *275*, 135–148.

(24) Kellogg, R. E.; Wyeth, N. C. *The Journal of Chemical Physics* **1966**, *45*, 3156–3158.

(25) Fleury, L.; Segura, J.-M.; Zumofen, G.; Hecht, B.; Wild, U. P. *Physical Review Letters* **2000**, *84*, 1148–1151.

(26) Banasiewicz, M.; Morawski, O.; Wiącek, D.; Kozankiewicz, B. *Chemical Physics Letters* **2005**, *414*, 374–377.

(27) Ringemann, C.; Schönle, A.; Giske, A.; Middendorff, C. v.; Hell, S. W.; Eggeling, C. *ChemPhysChem* **2008**, *9*, 612–624.

(28) Hu, D.; Yao, L.; Yang, B.; Ma, Y. *Philosophical Transactions. Series A, Mathematical, Physical, and Engineering Sciences* **2015**, *373*, 20140318.

(29) Kobayashi, S.; Kikuchi, K.; Kokubun, H. *Chemical Physics* **1978**, *27*, 399–407.

(30) Hoffman, D. P.; Shtengel, G.; Xu, C. S.; Campbell, K. R.; Freeman, M.; Wang, L.; Milkie, D. E.; Pasolli, H. A.; Iyer, N.; Bogovic, J. A.; Stabley, D. R.; Shirinifard, A.; Pang, S.; Peale, D.; Schaefer, K.; Pomp, W.; Chang, C.-L.; Lippincott-Schwartz, J.; Kirchhausen, T.; Solecki, D. J.; Betzig, E.; Hess, H. F. *Science* **2020**, *367*, DOI: 10.1126/science.aaz5357.

(31) Dahlberg, P. D.; Moerner, W. E. *Annual Review of Physical Chemistry* **2021**, *72*, 253–278.

(32) Hulleman, C. N.; Li, W.; Gregor, I.; Rieger, B.; Enderlein, J. *ChemPhysChem* **2018**, *19*, 1774–1780.